Journal of Optoelectronics and Advanced Materials Vol. 6, No. 2, June 2004, p. 511 - 521

INVITED PAPER

MAGNETIZATION PROCESS AND MAGNETIC LOSSES IN FIELD-ANNEALED AMORPHOUS AND NANOCRYSTALLINE RIBBONS

C. Appino, C. Beatrice, E. Ferrara, F. Fiorillo*

Istituto Elettrotecnico Nazionale Galileo Ferraris, Strada delle Cacce, 91 I-10135 Torino, Italy

The phenomenology of magnetization process and losses in amorphous and nanocrystalline ribbons and its dependence on the anisotropy induced by field annealing is presented and discussed for a wide range of measuring conditions. Attention is focused on the evolution of the domain structure with the direction (longitudinal/transverse) and intensity of the uniaxial macroscopic anisotropy K_u and the ensuing effects on the magnetization reversal mechanisms. Such an evolution is directly observed by means of Kerr effect experiments. It is shown that the balance between domain wall displacements and moment rotations determines shape and area of the quasi-static hysteresis loop, while imposing a specific dependence of the energy loss on the magnetizing frequency. With transverse domains, rotations predominantly contribute to the magnetization reversal, but the total energy losses can approach the correspondingly expected classical limit only when attaining the MHz range. Nanocrystalline ribbons realize the best combination of low losses and high permeability at all frequencies, but high permeability may eventually lead to skin effect. It is shown that, in all cases, the frequency dependence of the excess loss component follows a power law close to $f^{1/2}$, suffering from specific anomalies at high frequencies. The origin of such anomalies is envisaged as due to drifting balance between rotations and domain wall displacements, skin effects, and resonance phenomena.

(Received April 26, 2004; accepted June 3, 2004)

Keywords: Amorphous and Nanocrystalline Alloys, Induced Anisotropy, Magnetization Processes, Energy loss

1. Introduction

Nanocrystalline and near-zero-magnetostriction Co-based amorphous alloys display extremely soft magnetic properties and high versatile behavior, because the random frozen-in anisotropies are very low and can be easily overcome by macroscopic anisotropies K_u induced by field or stress annealing [1,2]. Besides having practical interest, as demonstrated by applications in a variety of sensors and devices, these properties offer unique opportunities in the investigation of specific features of the magnetization process, which can be settled to different regimes according to direction and intensity of the induced anisotropy. It is known in fact that, because of the low values of the anisotropies involved, irreversible domain wall displacements (DWD) and reversible rotations of magnetic moments (RMR) can comparably contribute to the magnetization reversal, their relative roles depending on factors like magnitude and direction of the macroscopic anisotropy K_u, distribution of frozen-in anisotropies, nucleation and coercive fields. By controlling K_u it is possible to shift the balance between these two processes and optimize the material performances, tailoring the hysteresis loop to specific applications. It is qualitatively known, for instance, that loop flattening by tranverse field annealing leads to low loss behavior at high frequencies in amorphous and nanocrystalline ribbons [3]. It has also been shown that this follows from RMR eventually prevailing over DWD, which implies a correspondingly decreasing effect on the excess loss

*Corresponding author: fiorillo@ien.it

component [4]. The associated phenomenology is, however, pretty complex and dependent, besides K_u, on a number of physical and geometrical parameters, like residual and applied stresses, material resistivity, and ribbon thickness.

In this paper we present and discuss representative results regarding domain structure, hysteresis loop, and magnetic energy losses from DC to 1 MHz in field-annealed near-zero magnetostriction amorphous alloys and nanocrystalline ribbons. We show that the induced macroscopic anisotropy K_u, competing with the local randomly distributed anisotropies, brings about with its variation a dramatic evolution of the domain structure, while controlling the respective roles played by DWD and RMR in both DC and dynamic regimes. This is put in evidence either by means of a detailed Kerr effect investigation, carried out on Co-based amorphous alloys under a wide range of longitudinal and transverse induced anisotropies, or by the measurement and analysis of the magnetic energy losses under quasi-static conditions and as a function of the magnetizing frequency. With the domain pattern evolving from longitudinal to transverse on increasing time and temperature of annealing under tranverse field, the hysteresis loop progressively flattens because, due to higher transverse K_u values, RMR increasingly contribute to the magnetization reversal. DWD, however, persist even with sharp transverse domains, chiefly in connection with domain nucleation and annihilation effects, and the hysteresis loop area (the quasi-static energy loss W_h) can consequently increase to a good extent. This has the important consequence that the medium-to-high frequency energy losses in flat-loop samples are, in spite of applied field nearly orthogonal to the 180° domain walls, still largely influenced by DWD, as signaled by the important contribution provided by the excess loss component W_{exc} to the total loss. Competition between DWD and RMR, taking place under dynamic conditions, eventually favors the latter at high frequencies, creating the conditions for attaining the sought-after classical limit W_{cl}. On approaching the MHz range, however, the conventional loss separation picture complicates to some extent, due to possible skin effect and resonance phenomena.

2. Experimental

We discuss experiments made on two different types of rapidly solidified alloys.

1) Near-zero-magnetostriction amorphous ribbons of composition $Co_{71}Fe_4B_{15}Si_{10}$ (thickness 18 μm, width 10 mm, saturation polarization J_s = 0.86 T) produced by the Planar Flow Casting technique in vacuum and subjected to thermal treatments under controlled atmosphere (either vacuum or argon).

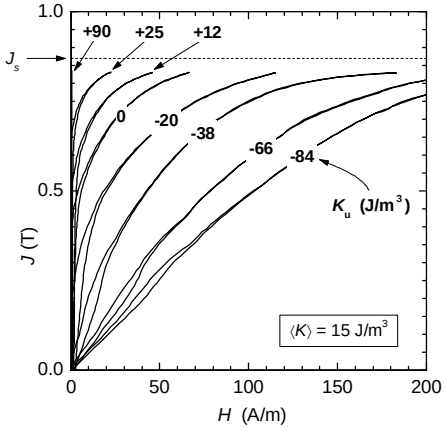

Fig. 1. $Co_{71}Fe_4B_{15}Si_{10}$ amorphous ribbons. Evolution of quasi-static hysteresis loops as a function of the induced anisotropy K_u (peak polarization J_p = 0.83 T). Corresponding evolution of the domain structure in the demagnetized state is shown in Fig. 2. Positive (negative) values of K_u indicate longitudinal (transverse) easy axis. Linearization of the loop with increasingly negative K_u values can be recognized. With transverse easy axis, the upper portion of the magnetization curve is covered almost exclusively by rotations and the material is nearly domain-free. At lower induction values domain wall processes take place and generate magnetic hysteresis. An example of such processes is provided, for K_u = -84 J/m^3, in Fig. 4.

Single strips and 30 mm diameter strip-wound ring samples were first annealed at 360 °C under longitudinal/circumferential saturating field (H = 1000 A/m), then subjected to sequential treatments under a transverse field ($H \cong$ 50 kA/m) at temperatures ranging between 200°C and 290°C. Following this procedure, a full range of K_u values, from longitudinal (LD, $K_u \sim +150$ J/m^3) to transverse (TD, $K_u \sim -84$ J/m^3) easy axis was obtained. Fig.1 illustrates the correspondingly obtained sequence of hysteresis loops for the ribbon samples.

2) Nanocrystalline $Fe_{73.5}Nb_3Cu_1Si_{13.5}B_9$ alloys, produced as 20 μm thick 10 mm wide ribbons by Planar Flow Casting in air. The as-quenched strip-wound ring samples were subjected to standard nanocrystallization treatment under transverse field $H \cong$ 50 kA/m at 520 °C – 540 °C in vacuum, followed by slow magnetic cooling. The resulting hysteresis loop was associated with a transverse easy axis, where the estimated K_u value ranged, in different samples, between -8 J/m^3 and -16 J/m^3.

The magnetic characterization of the so-prepared samples was carried out, under controlled sinusoidal induction waveform, starting from quasi-static regime (5 - 10 Hz), up to a maximum frequency of 1 MHz. A low-to-medium frequency testing (f < 10 kHz) was carried out in the range 0.005 T ≤ J_p ≤ 0. 83 T. At higher frequencies, the maximum investigated J_p value was 0.2 T. A digital hysteresisgraph-wattmeter endowed with a 200 W NF4025 power amplifier and a Tektronix TDS714L oscilloscope for synchronous acquisition and A/D conversion of the H and J signals was employed. For high frequency testing, measures were taken to ensure negligible effects from stray capacitances and inductances.

The domain structure and its evolution with the applied field were directly observed in the amorphous ribbons by means of a Kerr effect setup. The ribbons were mechanically polished and ZnS coated, in order to enhance optical contrast. The quality of the images was further improved by digital subtraction of the background image (i.e., saturated sample).

3. Results and discussion

3.1. Anisotropy and hysteresis loops

The experimental major hysteresis loops measured after field annealing can be associated, as shown in Fig. 1, with definite values of the induced macroscopic anisotropy K_u. Positive and negative K_u values in this figure stand for LD and TD macroscopic easy axis, respectively. K_u is estimated, together with the average frozen-in random anisotropy $< K >$, using a theoretical method directed at the prediction of the reversible portion of the DC magnetization curve on recoil from saturation. This coincides with the whole magnetization curve down to the point where domain nucleation starts, as apparent from branching of the curve due to hysteresis. The related physical model is described in Ref. [5]. It regards the specimen as an assembly of mesoscopic independent regions where, on progressively releasing the applied field H from the saturated state, the magnetization rotates according to the equilibrium between the torque imposed on it by the local anisotropy K, the macroscopic anisotropy K_u, and H. Neglecting grain-to-grain interaction fields and using standard statistical methods, the probability density function $p(\gamma)$ for the angle γ made in each region by the polarization vector J_s with LD is determined for any H value. Byintegrating over the range - π/2 ≤ γ ≤ π/2, the reversible magnetization along the recoil curve $J_{rev}^{(recoil)} = J_s \int_{-\pi/2}^{\pi/2} p(\gamma)\cos\gamma\, d\gamma$ is obtained.

3.2. Domain structure and magnetization process vs. induced anisotropy

The evolution of the hysteresis loop with field annealing, as reported in the example shown in Fig. 1 for the Co-based amorphous alloy, can be qualitatively understood looking at the evolution of the domain structure both as a function of the thermal treatment and along the magnetization curve. Fig. 2 provides an example of observed domain structure in the demagnetized state at various

stages of the field annealing sequence leading to the succession of loops in Fig. 1. The associated K_u values have been calculated as previously discussed. The related model predicts that the probability distribution function $p(\gamma)$ correspondingly evolves as shown in Fig. 3. The direct domain observation, the shape of the magnetization curves, and the calculated behavior of $p(\gamma)$ permit one to draw some general conclusion as to the nature of the magnetization process and its dependence on K_u.

In particular, three main phenomenological aspects of this process, depending on the relative strength of $< K >$ and K_u, can be roughly recognized.

1) $K_u > < K >$ (Fig. 2a). Under these conditions, a regular pattern of longitudinal domains exists. The magnetization proceeds almost exclusively by DWD and for sufficiently high K_u values the hysteresis loop is square-shaped.

2) $-< K > \leq K_u \leq < K >$ (Fig. 2b). On approaching this K_u range, the domain structure suffers a drastic change and a maze pattern appears, because of the random distribution of the local anisotropies. At the same time, the hysteresis loop shape becomes rounded.

3) $K_u < -< K >$ (Figs. 2c-2e). A transverse domain structure is formed, sharpening at higher negative values of K_u, and the hysteresis loop approaches a linear shape.

What we expect and quantitatively predict by the model on passing from longitudinal to transverse domain structure by means of field annealing, is that DWD are progressively superseded by RMR on providing the macroscopic magnetization reversal.

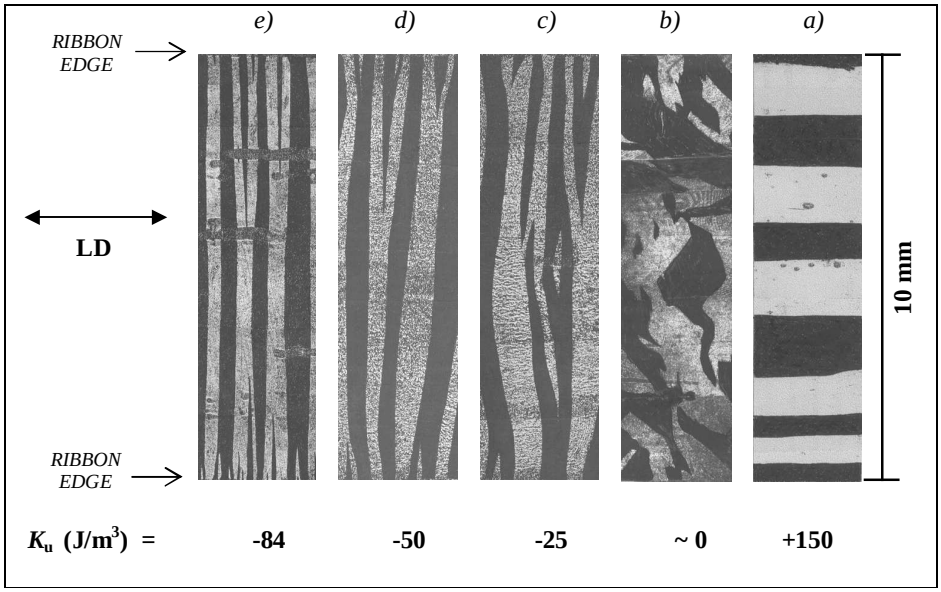

Fig. 2 - $Co_{71}Fe_4B_{15}Si_{10}$ amorphous ribbons. Domain structure in the demagnetized state as a function of the value of the macroscopic anisotropy constant K_u. The associated magnetization curves evolve as shown in Fig. 1. On passing from easy axis directed along LD ($K_u > 0$) to TD ($K_u < 0$), the distribution $p(\gamma)$ of the magnetization direction associated with the different domains changes from LD peaked to TD peaked, as illustrated by the calculations shown in Fig. 3. The maze domain structure observed with $K_u \cong 0$ is consistent with the assumed random distribution of the local anisotropies, having average modulus $< K >$.

The inset in Fig. 3 shows, as an example, the predicted evolution of the ratio J_{RMR} / J_p, the fractional contribution of reversible rotations to the total magnetization reversal J_p, as a function of K_u in the Co-based ribbon for $J_p = 0.2$ T. We see in this case, where J_p has a value of interest for high-frequency applications, that some domain wall activity persists even when K_u is sufficient to

create a relatively sharp transverse domain pattern (see Fig. 2). It turns then out that not only the quasi-static energy loss W_h correspondingly attains non-vanishing values, but also the excess loss component W_{exc}, directly associated with DWD, maintains an important role. W_h and W_{exc} are indeed related and hints at the high frequency behavior of the material can actually be induced from quasi-static measurements. Obviously, it is not the value of W_h that matters directly, because it becomes irrelevant at high frequencies, but the fact that it is a measure of the domain wall processes, that is of the difficulty of achieving the aimed at loss minimization.

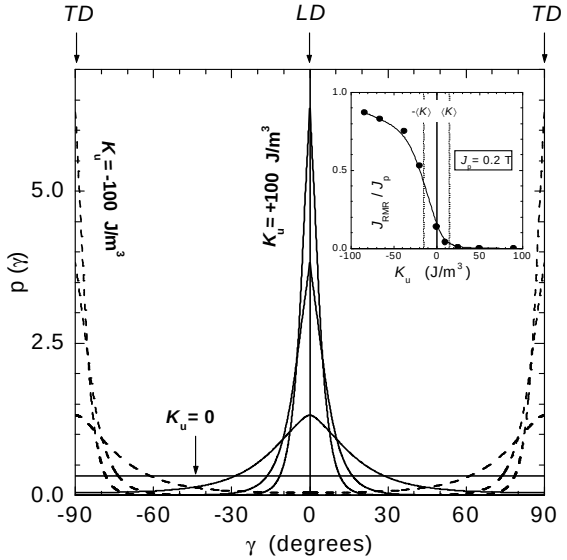

Fig. 3. Calculated evolution with K_u of the distribution function $p(\gamma)$ for the angle γ made in the demagnetized state by $\boldsymbol{J}_S$ with LD in the $Co_{71}Fe_4B_{15}Si_{10}$ amorphous ribbons ($\langle K \rangle$ ~15 J/m^3). The calculations have been made according to the model discussed in Ref. [5]. The different curves correspond to the following values of the macroscopic anisotropy: K_u = +100, +60, +20, 0 J/m^3 (solid lines), and K_u = -20, -60, -100 J/m^3 (dashed lines). The inset shows an example of correspondingly calculated ratio J_{RMR} / J_p, the fractional contribution provided by reversible rotations to the total magnetization reversal J_p.

Fig. 4 neatly illustrates the domain activity arising, under quasi-static conditions, in a Co-based amorphous ribbon with high transverse induced anisotropy (K_u = -84 J/m^3). The sequence of Kerr images follows, in particular, the domain nucleation, rearrangement, and annihilation processes taking place while traversing a major hysteresis loop between $\pm J_S$. We can observe domain nucleation events on arriving from the saturated state ($J_S = 0.86$ T) once we approach, by means of rotational processes, a polarization value $J \sim 0.7\, J_S$. The magnetization curve is evidently covered, in this magnetization interval, in a reversible fashion (see Fig. 1). Domain nucleation and growth processes proceed by decreasing the applied field, until a regular pattern is achieved in the demagnetized state. The driving force for domain structure creation and development is the demagnetizing field generated by the free poles at the ribbon edges and internal imperfections. These arise from the rotation of the magnetization towards the easy axis and domain creation is the obvious process leading to decrease of the magnetostatic energy. We estimate, by approximate calculation of the magnetostatic energy, taking into account the μ*-effect [6], a nucleation field of the order of few A/m for J = + 0.6 T (see Fig. 4). Once the demagnetized state has been left behind by application of a negative field, the decrease of the magnetostatic energy by rotation of the moments towards LD progressively leads to domain annihilation, in a somewhat specular way with respect to domain nucleation and growth.

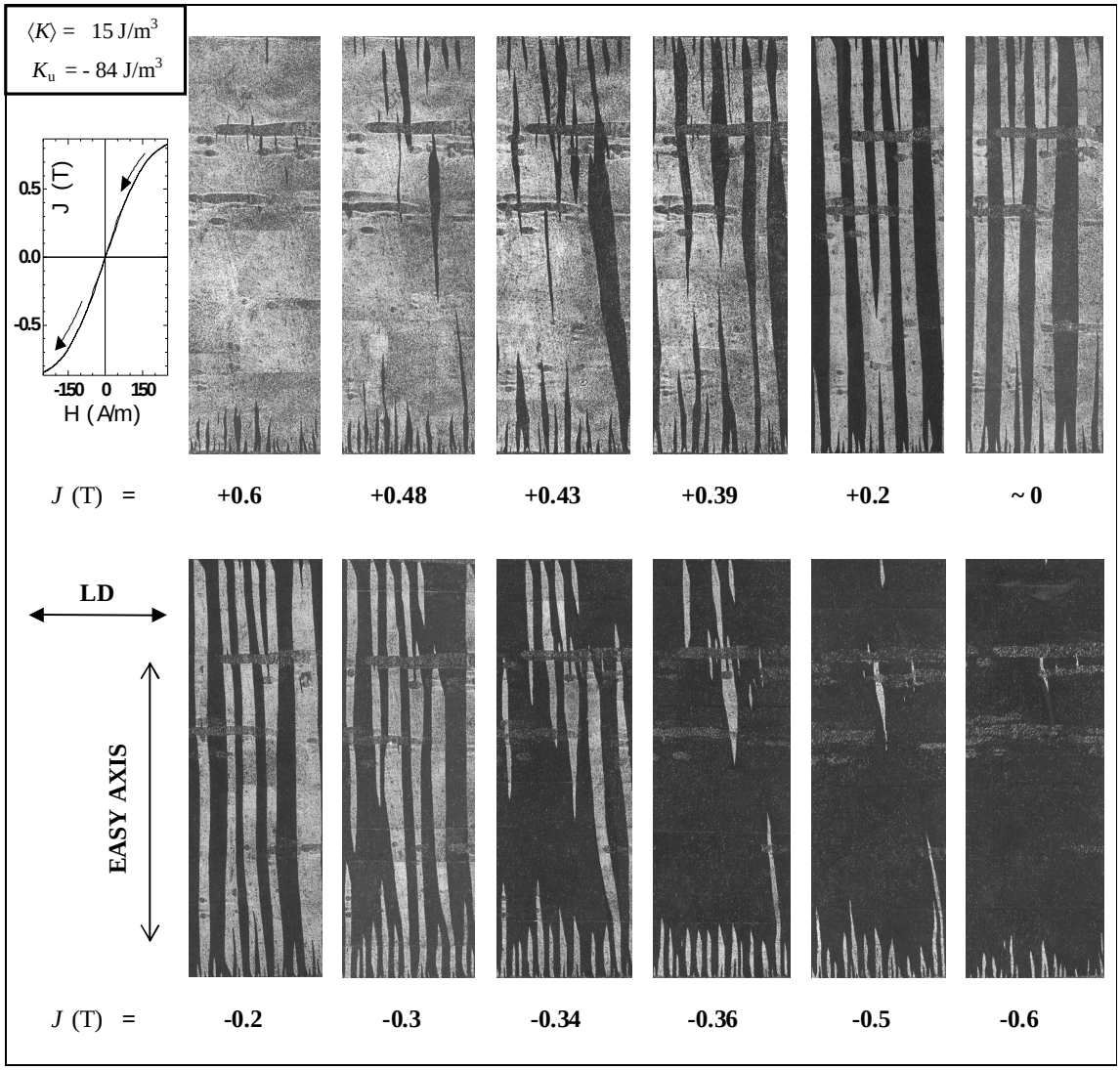

Fig. 4 – $Co_{71}Fe_4B_{15}Si_{10}$ amorphous ribbons. Domain structure evolution along a branch of a major hysteresis loop in a sample endowed with transverse easy axis (K_u = -84 J/m^3, <K> ~ 15 J/m^3). Rotation of the magnetic moments, either towards or away from the easy axis under changing applied field brings about a change of the free pole distribution at the ribbon edges and internal defects. Domain nucleation, rearrangement, and annihilation processes are therefore chiefly driven by the ensuing magnetostatic effects.

Having in mind this kind of observations, made at different K_u values, we can qualitatively understand the dependence of the DC energy loss W_h (obtained by extrapolating to zero frequency the total energy loss W vs. f curve) on K_u. Experimental results obtained in the Co-based amorphous alloy are shown in Fig. 5. Remarkably, on decreasing K_u from positive to negative values (i.e., from longitudinal to transverse easy axis), which implies increasing the rotational contribution J_{RMR}, W_h is found to increase, whatever J_p. It attains a maximum value for slightly negative K_u (that is, for K_u around $-<K>$). These results point to specific coercivity mechanisms involved with different domain topologies, as partially illustrated in Fig. 2 and Fig. 4.

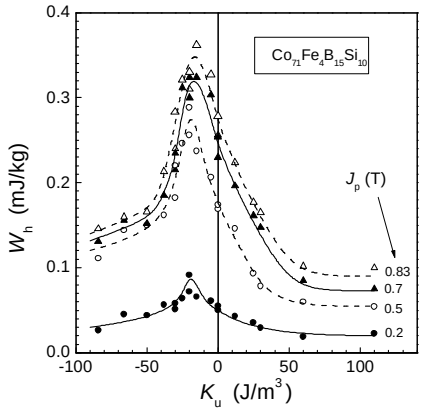

Fig. 5. $Co_{71}Fe_4B_{15}Si_{10}$ amorphous ribbons. Hysteresis loss W_h vs. macroscopic uniaxial anisotropy K_u at different peak polarization values.

We can schematically refer, looking also at Fig. 3, to the previously discussed regions of variation of K_u.

1) $K_u > < K >$. In this region, where a longitudinal easy axis is present, the magnetization reversal chiefly occurs through displacements of rigid plane 180° walls and W_h tends to vary, according to specific pinning mechanisms, as $K_u^{1/4} - K_u^{3/4}$ [7,8].

2) $- < K > \leq K_u \leq < K >$. In this K_u range, where a maze domain structure is observed, the walls become flexible and one- and two-dimensional vaulting can occur. With flexible walls, pinning is more effective, coercivity increases on approaching K_u =0 approximately like $< K > / \sqrt{K_u + < K >}$ [9], and the same occurs to W_h, in spite of an increased proportion of RMR. On passing to negative K_u values, a further increment of W_h is initially expected, because of the increasing role of domain nucleation and rearrangement processes.

3) $K_u < - < K >$. In this region W_h eventually decreases with increasing the value of the transverse anisotropy. The walls become rigid again, the transverse domain pattern is stabilized quickly upon nucleation (weakened μ^*-effect) and coherent spin rotations increasingly contribute to the magnetization reversal along LD (inset in Fig. 3). The present results indicate, however, that vanishing hysteresis loss might be reached at such high values of transverse K_u that permeability would be uninterestingly small.

To remark that in nanocrystalline alloys the physical mechanism operating during field annealing, likely associated with the magnetic ordering in the Fe-Si phase, is much weaker than in the amorphous alloys and the available K_u range is consequently more limited. It appears, however, that $< K >$ can be made very small (say ~ 1 – 2 J/m^3), so that important and predominant RMR processes can always take place in transverse field-annealed samples, at least at low J_p values (e.g., J_p < 0.2 T), and the associated permeability is high. For the here-investigated FINEMET type alloy, we find, for example, that a relative DC initial susceptibility of the order of $4 \cdot 10^4$, mostly due to RMR, can be obtained. This expectedly reflects into a largely reduced excess loss with respect to the amorphous alloys and a generally improved high-frequency behavior.

3.2. Energy loss vs. magnetizing frequency

We have previously stated that, in order to achieve excellent material behavior at high frequencies, RMR processes should contribute for the most part to the magnetization reversal. This

would minimize the excess loss component W_{exc}. It has been hinted further that the quasi-static energy loss W_h should in any case be small, not only for its direct contribution to the dynamic loss, but also for its direct relationship with the excess loss. We may clarify these statements by means of few illustrative results, encompassing a wide frequency range.

To start with, let us examine in Fig. 6 the frequency dependence up to 1 MHz of the total energy loss measured at J_p = 0.02 T in differently treated amorphous and nanocrystalline ring samples. They are: 1) Amorphous magnetostrictive $Fe_{78}B_{13}Si_9$ alloy in the as-quenched state; 2) Amorphous near-zero magnetostriction $Co_{71}Fe_4B_{15}Si_{10}$ alloy, in the as-quenched state; 3) The same alloy after transverse field annealing (K_u ~ -50 J/m^3); 4) Nanocrystalline $Fe_{73.5}Nb_3Cu_1Si_{13.5}B_9$ alloy, after transverse field annealing (K_u ~ - 10 J/m^3). Sample 1) is endowed with high magnetostriction and in the as-quenched state the frozen-in random anisotropy $< K >$ is typically of the order of few hundred J/m^3. Additional anisotropy effects are expectedly induced by ribbon bending into the ring specimen radius. Both RMR and DWD take place in samples 1), 3), and 4), while in sample 2), characterized by a longitudinal bar-like domain structure the magnetization process can only proceed by DWD. It is noted that the loss in this sample eventually becomes the largest at high frequencies.

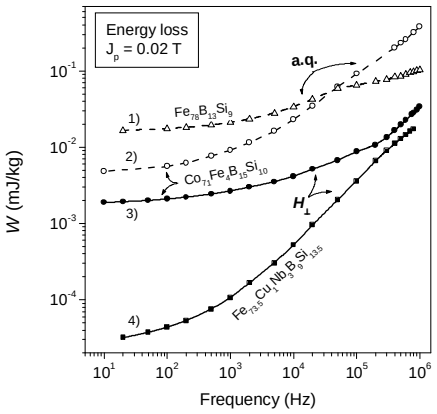

Fig. 6. Total energy loss vs. magnetizing frequency in different rapidly solidified alloys, all tested at J_p = 0.02 T as 30 mm diameter strip-wound ring samples (ribbon width 10 mm, thickness 18 μm - 20 μm). The reported results refer to the following compositions: 1) Amorphous magnetostrictive $Fe_{78}B_{13}Si_9$ alloy in the as-quenched (a.q.) state; 2) Amorphous near-zero magnetostriction $Co_{71}Fe_4B_{15}Si_{10}$ alloy, in the as-quenched state; 3) The same alloy after transverse field annealing (K_u ~ -50 J/m^3); 4) Nanocrystalline $Fe_{73.5}Nb_3Cu_1Si_{13.5}B_9$ alloy, after transverse field annealing (K_u ~ -10 J/m^3). Open symbols and dashed lines correspond to as-quenched samples. Solid symbols and lines correspond to samples annealed under transverse field.

These results, which are qualitatively reproduced also for the other investigated J_p values, can be put under rational perspective exploiting the concept of loss separation. Fig. 7 illustrates the loss separation procedure up to 1 MHz in the amorphous $Co_{71}Fe_4B_{15}Si_{10}$ samples 2) and 3). Here the hysteresis, excess, and classical loss components have been represented according to the equation $W = W_h + W_{exc} + W_{cl}$. The basic point conveyed by this measurement is that the difference in the high frequency loss displayed by the two samples induced by the thermal treatment they have been subjected to, is almost totally due to the different behavior and amplitude of the excess loss W_{exc}. We notice, in particular, that in the as quenched sample 2), where only DWD occur, W_{exc} follows a defined power law dependence on frequency ($W_{exc} \propto f^{0.6}$) up to 1 MHz. In the transversally annealed sample, where DWD and RMR both contribute to the magnetization process, W_{exc} follows

this dependence ($W_{exc} \propto f^{0.5}$) only in the low-to-medium frequency range. It then exhibits a reduced rate of increase with *f*, ending into a plateau, to rise again briskly on approaching the MHz region. Looking at the overall behavior of W_{exc} vs. *f* in the tested samples shown in Fig. 8, we see that a similar plateau by W_{exc} is found in the as- quenched $Fe_{78}B_{13}Si_9$ amorphous ribbon, and it is barely detectable in the $Fe_{73.5}Nb_3Cu_1Si_{13.5}B_9$ nanocrystalline alloy. Apparently, some eddy current mechanism is here at work, where the role of DWD is constrained in favor of RMR, so that the classical limit is approached quickly.

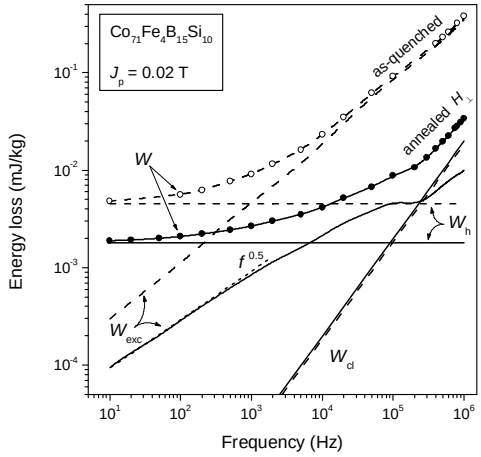

Fig. 7. Example of loss separation ($W = W_h + W_{exc} + W_{cl}$) in the near-zero magnetostriction $Co_{71}Fe_4B_{15}Si_{10}$ amorphous alloy. Open dots and dashed lines: as-quenched state, characterized by longitudinal bar-like domain structure and magnetization process by DWD. Solid dots and continuous lines: after stress relaxation annealing and transverse field annealing ($K_u \sim$ -50 J/m^3). The domain structure is transverse (see Fig. 2) and the magnetization proceeds by DWD and RMR. The symbols denote the measured total loss *W*.

A power law dependence of W_{exc} on *f* is what we expect from the statistical theory of losses [10]. This theory therefore fully applies to results in sample 2) and, over a more or less extended frequency range to the other samples, independent of the relative proportions of DWD and RMR. In the latter case, we should explicitly take into account, however, that a good wide part of the magnetization reversal is accomplished by reversible rotation processes. By phenomenologically introducing the ratio $R_{dwd} = J_{dwd} / J_p$, which defines the fractional contribution to J_p provided by DWD, we write the excess loss as [4]

$$W_{exc}(f) = 8 J_p^3 \sqrt{\sigma G_X V_o R_{dwd}^3 f} \tag{1}$$

where G_X is a generalized wall damping coefficient, σ is the material conductivity, and V_o is a statistical parameter related to the distribution of the domain nucleation and domain wall pinning fields. This equation makes quantitative the idea that the dependence of W_{exc} on *f* is modulated by the dependence of the ratio R_{dwd} on *f*. If R_{dwd} is to decrease with increasing frequency, which is what we expect to happen, sooner or later, when DWD are associated with RMR, the same occurs to the rate of increase of W_{exc}. This apparently occurs in the present samples 1), 3), and 4), although, as shown in Fig. 8, the detailed circumstances can differ from sample to sample.

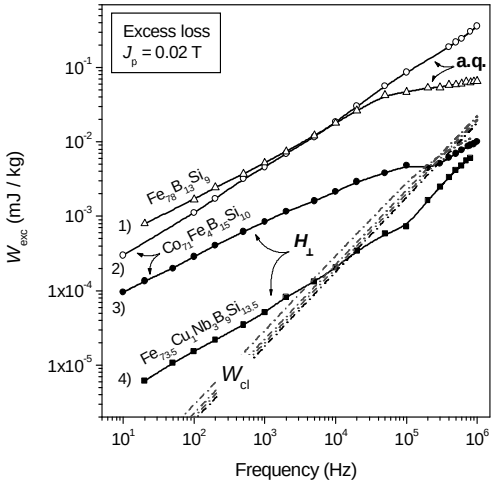

Fig. 8. Excess and classical (dotted lines) energy loss components vs. magnetizing frequency in the investigated materials. The excess loss always follows a power law dependence on frequency $W_{exc} \propto f^n$, with n ~ 0.5 – 0.6 in the low-medium frequency range. At high frequencies, drifting balance between DWD and RMR may bring about a reduced rate of increase of W_{exc} with f, possibly compounding with further anomalies on approaching the MHz range. Similar results are obtained with the other investigated J_p values (ranging between 0.005 T and 0.2 T). Open symbols correspond to as quenched samples. Solid symbols correspond to samples annealed under transverse field.

From a general viewpoint, we expect that DWD will be more effectively damped by eddy currents than RMR on increasing the magnetizing frequency. It is reasonable to assume, in fact, that, under dynamic conditions, DWD will be resisted both by the local eddy current fields (excess field $H_{exc} \cong W_{exc} / 4J_{dwd}$), generated on the scale of the magnetic domains, and the field generated by the long range eddy currents (classical field $H_{cl} \cong W_{cl} / 4J_p$), while RMR will be contrasted only by the latter. It turns then out that the balance between the applied field and all internal static and dynamic counterfields (associated with anisotropy, coercivity, and eddy currents) will be shifted in such a way as to drive RMR further, at DWD's expense. The ratio R_{dwd} will decrease and, according to Eq. (1) the increase of W_{exc} with f will slow down. We will expectedly observe this effect at those frequencies where the value of H_{exc} is high enough to compare with the fields required to drive appreciable rotation of the magnetic moments against the anisotropy. A process of this kind should clearly accelerate the achievement of the classical limit, but, the approach to such a limit in the MHz range might become an elusive matter. This is demonstrated by the appearance of a somewhat abnormal surge of W_{exc} beyond some 100 kHz in samples 3) and 4). Two possible sources for this high-frequency extra contribution to the loss are envisaged. First, skin effect does affect W_{exc}, leading in particular to an increase of it with frequency (the effect on W_{cl} has been already calculated in the results shown in Figs. 7 and 8). Flux penetration is indeed far from complete in the present nanocrystalline alloys (thickness 20 μm, initial permeability $\mu_r \cong 40 \cdot 10^3$) beyond few hundred kHz (skin depth around 4 μm at 1 MHz). Second, additional losses should possibly be provided by resonant absorption associated with spin rotation. According to Snoek's model, the resonant frequency is $f_o = \dfrac{\gamma_e J_s}{3\pi\mu_r}$, with $\gamma_e = 1.76 \cdot 10^{11}$ $T^{-1}s^{-1}$ the electron gyromagnetic ratio. In the nanocrystalline alloys, where J_s = 1.23 T, we obtain f_o ~ 500 kHz, while for the Co-based alloys, where J_s = 0.86 T and $\mu_r \cong 4.3 \cdot 10^3$, we obtain f_o ~ 3.3 MHz. Conclusive evidence as to the nature and role of the various energy loss contributions in the amorphous and nanocrystalline alloys in the

MHz range actually needs further experimental work, aimed at enlarging the set of the here considered physical and geometrical parameters. This will be the subject of further investigation.

4. Conclusions

Co-based amorphous and nanocrystalline alloys can have their magnetization curve linearized and their magnetic energy losses minimized when transverse anisotropy is induced by convenient field annealing treatment. The ensuing transverse domain pattern is conducive to a magnetization process where reversible rotations of the magnetic moments (RMR) are largely prevalent over irreversible domain nucleation and wall displacement processes (DWD). Detailed Kerr effect investigations show, however, that DWD always come along, as they are chiefly connected with the condition of minimum magnetostatic energy at the ribbon sample edges. Persisting DWD are the source of excess losses and the envisaged limiting loss condition, where only classical loss survives, can be approached only beyond some 10 kHz in nanocrystalline ribbons and 100 kHz in amorphous ribbons. In some cases, the transition to the classical regime is accelerated, the DWD giving way to RMR because of increasingly unfavorable eddy current patterns. However, on approaching the MHz range, skin effects and resonances can be the source of additional losses.

References

[1] K. Zàveta, O.V. Nielsen, K. Jurek, J. Magn. Magn. Mater. **117**, 61 (1992).
[2] Y. Yoshizawa , K. Yamauchi, IEEE Trans. Magn. **25**, 3324 (1989).
[3] G. Herzer, Phys. Scripta **T20**, 22 (1988).
[4] C. Appino, C. Beatrice, E. Ferrara, F. Fiorillo, J. Magn. Magn. Mater. **254-255**, 213 (2003).
[5] C. Appino, F. Fiorillo, J. Appl. Phys. **76**, 5371 (1994).
[6] A. Hubert, R. Schäfer, *Magnetic domains* (Springer, Berlin, 1998), pp. 130.
[7] H. Kronmüller, B. Gröger, J. Phys. (Paris) **T42,** 1285 (1981).
[8] J. L. Porteseil, O. Geoffroy, J. Magn. Magn. Mater. **140-144**, 1855 (2003).
[9] L. Néel, Ann. Univ. Grenoble **22**, 299 (1946).
[10] G. Bertotti, IEEE Trans. Magn. **24**, 621. (1988).